Knockdown of muscle-specific Ribosomal Protein L3-Like enhances muscle function in healthy and dystrophic mice

Betty R. Kao[1]*, Alberto Malerba[1]*, Ngoc B. Lu-Nguyen[1], Pradeep Harish[1], John J. McCarthy[2], George Dickson[1], Linda J. Popplewell[1]†

1. Department of Biological Sciences, School of Life Sciences and the Environment, Royal Holloway University of London, Egham, Surrey, TW20 0EX, UK

2. University of Kentucky, Lexington, Kentucky, United States

* The first 2 authors equally contributed to the manuscript

† Correspondence should be addressed to L.J.P.

Dr Linda Popplewell,

Department of Biological Sciences,

School of Life Sciences and the Environment,

Royal Holloway University of London,

Egham, Surrey, TW20 0EX, UK.

Tel: +44 (0)1784-443980

Fax: +44 (0)1784 414224

Email: linda.popplewell@rhul.ac.uk

Short title: Ribosomal protein knockdown improves muscle force

Abstract

Ribosomal protein L3-Like (RPL3L) is a poorly characterised ribosomal protein that is exclusively expressed in skeletal and cardiac muscle. RPL3L is also downregulated in Duchenne muscular dystrophy, suggesting it may play an important role in muscle biology. Here, we investigated the role of RPL3L in skeletal muscle of healthy C57 and dystrophic *mdx* mice. We show that RPL3L is developmentally regulated and that intramuscular AAV-mediated RPL3L knockdown in the tibialis anterior of C57 and *mdx* mice results in increased specific force with improved resistance to eccentric contraction induced muscle damage in dystrophic muscles. The mechanism by which RPL3L knockdown improves muscle function remains unclear. Histological observations showed a significant increase in muscle length and decrease in muscle cross sectional area after RPL3L inhibition suggesting that this ribosomal protein may play a role in myofibre morphology. The endogenous downregulation of RPL3L in Duchenne muscular dystrophy may be a protective mechanism that attempts to improve skeletal muscle function and counteract the dystrophic phenotype.

Keywords

Duchenne muscular dystrophy, gene therapy, ribosomal protein, muscle function, *in vivo* muscle electrophysiology

Introduction

Ribosomal protein L3-like (RPL3L) is a poorly characterised ribosomal protein that shares 74% homology with its paralogue RPL3, a highly conserved ribosomal protein essential for peptidyltransferase activity[1, 2]. RPL3L and RPL3 are two of up to eighty ribosomal proteins and four ribosomal RNA molecules that constitute the eukaryotic ribosome, the translational machinery that generates protein from the mRNA template[3]. These two ribosomal proteins display mutually exclusive tissue-specific expression; RPL3L is exclusively expressed in cardiac and skeletal muscle while RPL3 is ubiquitously expressed at high levels, except in cardiac and skeletal muscle[4]. This tissue-specific expression of RPL3L is striking given that very few ribosomal proteins show tissue-specificity[5] and is therefore suggestive of a crucial role in muscle. Recently it has been shown that RPL3L expression is essential for correct function in the heart[6]. It has been reported that RPL3L is downregulated following hypertrophic stimulus, and overexpression of RPL3L in cultured murine C2C12 myogenic cells resulted in impaired myotube fusion[7]. These data together suggest the hypothesis that RPL3L is a negative regulator of skeletal muscle growth[7].

Several transcriptomic studies have found RPL3L to be downregulated in Duchenne muscular dystrophy (DMD)[8-10], a fatal muscle wasting disorder affecting 1 in 5000 boys[11]. DMD is caused by mutations in the *DMD* gene that result in the absence of the dystrophin protein, an integral component of the dystrophin-glycoprotein complex which connects muscle fibres to the surrounding extracellular matrix[12]. Dystrophin interacts with many structural and signalling molecules at the muscle sarcolemma hence its absence causes disruptions in multiple networks leading to a complex molecular pathophysiology that remains poorly defined and understood[13]. This has hindered efforts to develop treatments for DMD. To treat the underlying cause of DMD, dystrophin protein needs to be expressed. A promising dystrophin restoration approach is gene therapy using micro-dystrophin. This approach has been

successful in numerous animal and preclinical studies and has now entered clinical trials in patients[14].

This manuscript presents the first investigation into the role of RPL3L in skeletal muscles of healthy (C57) and dystrophic (*mdx*) mice. We investigated the developmental expression of RPL3L, we knocked-down and overexpressed RPL3L in the tibialis anterior (TA) muscle via intramuscular injection of an adeno-associated virus (AAV) carrying an shRNA targeting RPL3L or RPL3L expression vector respectively and examined the effects on muscle function. Whilst AAV mediated RPL3L transgene expression did not increase protein expression likely due to unknown compensatory effects, RPL3L knockdown significantly downregulated the protein and improved muscle strength in both C57 and *mdx* mice. These findings show that RPL3L is important for skeletal muscle function and that its knockdown in this tissue could potentially alleviate some of the muscle force deficit observed in DMD.

Results

RPL3L and its paralogue RPL3 are developmentally regulated in skeletal muscle

To investigate the developmental expression of RPL3L and its paralogue RPL3, Western blot analysis was performed using tibialis anterior (TA) muscles from C57 and *mdx* mice aged 1 day, 3 days, 7 days (1 week), 14 days (2 weeks) and finally 56 days old (8 weeks). RPL3L protein expression was up to 10.8-fold lower in 1 week old *mdx* compared to C57 mice (p=0.041, **Figure 1A, B**) consistent with previous studies that showed RPL3L mRNA is significantly downregulated in dystrophin-deficient muscle[8-10]. We also observed that RPL3 protein expression was up to 4.1-fold higher in 8-week old *mdx* compared to C57 mice (p=0.0174, **Figure 1A, C**). This dataset displaying an inverse relationship in protein expression of RPL3L and RPL3 suggests strong post-natal developmental regulation. To assess where in the myofibres RPL3L protein is expressed, we analysed TA muscles of 4 and 8-week old C57

and *mdx* mice through immunohistochemical staining of prepared cryosections. At these stages, myofibres in C57 muscles show a compact, organised structure with no central nucleation and a small amount of fibrotic tissue (**Figure 1D** and **Supplementary figure 1**). On the contrary, in dystrophic muscles of 4-week old mice several clusters of small centrally nucleated fibres are observed together with large areas of fibrotic tissue (**Figure 1D** and **Supplementary figure 1)**. In TA muscles of 8-week old *mdx* mice, a significant reduction in regeneration and fibrosis was detected relative to C57 TA muscle (**Figure 1D** and **Supplementary figure 1)**. RPL3L protein was detected at both time points in all muscles analysed mainly in the subsarcolemmal region or at the level of sarcolemma (**Figure 1D**). In TA muscles of 4 week old *mdx* mice only the large myofibres stained positive while clusters of small regenerating myofibres did not express RPL3L (**Figure 1D**) for RPL3L, suggesting that the reduction in protein expression displayed by *mdx* muscles may be due, at least partially, to the lack of expression in the smaller regenerating fibres. In TA muscles of 8 week old C57 and *mdx* mice all fibres express the protein although lower expression was detected in *mdx* muscles.

RPL3L overexpression does not affect muscle function while its knockdown significantly improves muscle function in C57 and mdx mice

To determine the function of RPL3L in skeletal muscle, we tried to either overexpress or knock down RPL3L in the TA muscle of C57 and *mdx* mice. Specifically 5 x 10^{11} viral particles of AAV-9 encoding a transgene to overexpress RPL3L (AAV-RPL3L) or 5 x 10^{10} viral particles AAV9 encoding a shRNA to knockdown RPL3L (AAV-shRPL3L) were injected into the left TA, with the contralateral muscle injected with an equal volume of saline in 8 C57 and 6 *mdx* mice at 6 weeks of age. Seven weeks after injection, TA muscle function was assessed by *in vivo* muscle electrophysiology and the muscles were harvested. Expression of RPL3L construct

in C57 and *mdx*, was confirmed by Western blot analyses as suggested by HA tag expression (**Supplementary figure 2A**). However this did not result in RPL3L protein overexpression (**Supplementary figure 2A-B**), neither in significant changes in maximal tetanic or maximal specific force neither in resistance to eccentric contractions (**Supplementary figure 2C-E**). Accordingly, muscle length, muscle mass and muscle cross sectional area (CSA) were also not significantly affected (**Supplementary figure 2F-M**). On the contrary, muscle electrophysiological analysis revealed a significant improvement of muscle strength and resistance to fatigue in C57 and *mdx* mice following RPL3L knockdown. RPL3L knockdown in C57 mice showed a significant 1.20-fold increase in specific force ($p=0.039$, **Figure 2A**), while in *mdx* mice AAV-shRNA treatment resulted in a significant 1.45-fold increase ($p=0.033$) (**Figure 2B**). RPL3L knockdown conferred a protective effect against eccentric contraction induced damage (normally seen in dystrophic muscle[15, 16]) with treated muscles showing greater resistance compared to control dystrophic muscles (keeping at least 1.7 folds the resistance of control muscles from the 5^{th} to the last contraction, $p<0.001$ to $p<0.05$, **Figure 2C**).

Analysis of TA muscles showed successful knockdown of RPL3L in the C57 and *mdx* mice compared to controls (**Figure 3A-D**) with significant reduction in RPL3L protein expression to 21.70% ± 0.04% of control levels in C57 mice ($p=0.0063$, **Figure 3A, B**) and 27.90% ± 0.02% of control levels in *mdx* mice ($p=0.013$, **Figure 3C, D**). Significant protein inhibition was also observed by immunofluorescence in both C57 and *mdx* muscles (**Figure 3E, F**)**.**

No significant differences were observed in TA mass of either C57 ($p=0.60$) or *mdx* ($p=0.22$) muscles between control and knockdown groups (data not shown). No difference was observed for the TA cross sectional area of whole C57 muscles treated with shRNA or saline (**Figure 3G**), but TA cross-sectional area significantly decreased in *mdx* mice ($p=0.026$) (**Figure 3H**). Myofibre CSA reduction in both C57 and *mdx* mice was not significant (**Figure 3I, L**),

although the difference in *mdx* mice was larger and closer to achieving significant difference (11.80% ± 0.04% decrease in mean fibre area, p=0.07), (**Figure 3L**). Notably, TA length was significantly longer following RPL3L knockdown in both C57 (p=0.007, **Figure 3M**) and in *mdx* mice (p=0.033, **Figure 3N**). Since RPL3L knockdown significantly improved muscle force in *mdx* mice, we assessed the percentage of centrally nucleated fibres (CNF) and the fibrotic tissue deposition. However, neither the percentage of CNF (**Supplementary figure 3A, B**) or the area covered by collagen VI or stained by sirius red (**Supplementary figure 3A, C-E**) significantly changed in muscles where RPL3L is knocked down compared to saline treated controls. These data suggest that while RPL3L overexpression does not affect muscle function and morphology, its inhibition significantly changes muscle shape and increases skeletal muscle strength. The improvement in muscle force is not due to changes in myofibre nucleation or fibrotic tissue deposition.

Discussion

Our data confirmed that RPL3L and its paralogue RPL3 are developmentally regulated and display an inverse relationship. Low expression of RPL3L and high expression of RPL3 coincides with rapid muscle growth during the neonatal period whilst high expression of RPL3L and low expression of RPL3 occurs once the rate of growth slows down in adulthood. Accordingly, we found that the clusters of small regenerating fibres usually detectable in large numbers in muscles of dystrophic mice at very young age do not express RPL3L. Once the tissue degeneration-regeneration processes slow-down and myofibres achieve a more mature stage, RPL3L is expressed by all myofibres. These observations are consistent with previous work by Chaillou et al. who reported that RPL3L is downregulated and RPL3 is upregulated in processes leading to hypertrophy. In response to a hypertrophic stimulus higher number of myogenic cells, where RPL3L is downregulated, fuse with the pre-existing fibres to increase

the muscle size. The authors showed that induction of RPL3L expression impairs myotube growth and myoblast fusion and proposed that RPL3L is a negative regulator of muscle growth[7]. However, we did not observe a significant increase in TA mass or CSA following RPL3L knockdown. On the contrary, a significant increase in myofibre length was observed. These data suggest that even though RPL3L is downregulated in hypertrophy[7], this is not caused by RPL3L knockdown *in vivo* at least when the protein inhibition is performed postnatally.

Given that RPL3L is expressed during periods of slow growth and the hypothesis that RPL3L is a negative regulator of muscle growth[7], it is possible that RPL3L is responsible for slower translation of muscle-specific mRNA transcripts, compared to RPL3. Following from this hypothesis, downregulation of RPL3L would result in upregulation of muscle-specific proteins. Techniques such as polysome and ribosome profiling are required to confirm this. These experiments were not feasible in this study due to the limited quantity of AAV-injected muscle, but this could be overcome by generation of an RPL3L-knockout mouse.

The most striking result of this study was that RPL3L knockdown enhanced muscle function in both C57 and *mdx* animals. This is somehow expected if RPL3L is a true negative regulator of muscle growth, as already observed for example for myostatin[17]. It has been shown in multiple studies that while myostatin, a member of the TGFβ family and negative regulator of muscle growth, is indeed downregulated in dystrophic muscles[18], its further inhibition improves muscle pathology, in particular once a parallel treatment to restore dystrophin is provided[19-22]. This is further confirmed by the observation that RPL3L overexpression in dystrophic muscles resulted in neither significant improvement nor impairment of muscle function that also leads to the conclusion that the downregulation of RPL3L in DMD does not contribute to the DMD pathophysiology.

It is possible that downregulation of RPL3L is a protective mechanism triggered to try and improve muscle function in dystrophic conditions that, however, is not sufficient to counteract the many layered effects and complex pathophysiology of dystrophin-deficiency. Therefore, a further knockdown of RPL3L by AAV-shRPL3L injection is beneficial to improve muscle function in *mdx*. These results suggest that RPL3L inhibition could be used as a therapeutic strategy for treatment of skeletal muscles in DMD. Related to this, it would be interesting to analyse the RPL3L expression in dystrophic cardiac muscle as well since a correct expression of RPL3L is important to maintain the functionality of the cardiac muscle[6]. Furthermore, it would be interesting to examine the levels of RPL3L in other muscular dystrophies to verify is a similar RPL3L endogenous downregulation exists.

As expected, due to the short time point used in our experiments, RPL3L knockdown did not result in change in fibrosis deposition or myofiber central nucleation. However we cannot exclude that, in the long term, RPL3L reduction could affect muscle regeneration processes. RPL3L knockdown resulted in a significant increase in TA length in both C57 and *mdx*. Although there are no reported links between increased muscle length and increased specific force, there is however a link between decreased sarcomere length and decreased specific force[23]. We speculate that RPL3L knockdown can affect sarcomeres in such a way as to improve muscle function possibly affecting the muscle-specific translation of proteins determinant of sarcomere length, like titin[23]. This is indeed a long protein that may need a quick translation, like the one provided by RPL3 that is supposed to be up-regulated when RPL3L is inhibited. It remains unclear how resistance to eccentric contraction-induced damage in *mdx* is improved. In summary, we show that RPL3L knockdown can enhance muscle function in healthy muscles and propose that endogenous RPL3L downregulation seen in DMD is a protective mechanism and attempt to enhance muscle function and counteract the dystrophic phenotype.

Materials and methods

Generation of AAV plasmid constructs and vectors

shRNA sequences to knockdown RPL3L were designed by Benitec Biopharma and packaged into a mammalian shRNA knockdown vector driven by a U6 promoter with a GFP reporter (VectorBuilder). Knockdown was tested empirically in Human Embryonic Kidney cells (HEK293T, ATCC, Manassas, USA) co-transfected with a vector expressing RPL3L to determine the shRNA sequence that yielded maximum RPL3L knockdown (designated as shRPL3L: GAAACATCTGGAGAAAGAGAA).

Cell culture and AAV preparation

HEK293T cells were grown in Dulbecco's modified Eagle's medium containing 10% fetal bovine serum, 20 mM HEPES and 2 mM glutamine in a humidified 5% CO_2 air atmosphere at 37°C. For vector preparation, a double transfection protocol was used as previously described[24]. Briefly, HEK293T cells were cultured in roller bottles and transfected with the AAV-shRPL3L knockdown plasmid and the pDP9rs AAV serotype 9 helper plasmid using polyethylenimine at a ratio of 1:4. After 72 hours incubation, cells were lysed and viral particles were precipitated using polyethylene glycol-2000 and purified using iodixanol step-gradient ultracentrifugation. The viral titre was determined relative to a plasmid DNA standard using real-time qRT-PCR with primers targeting the EGFP marker of the shRNA construct (AGCAGCACGACTTCTTCAAGTCC and TGTAGTTGTACTCCAGCTTGTGCC) and primers targeting the AAV polyA region of the shRNA construct (GAGTTTGGACAAACCACAAC and CCCCCTGAACCTGAAACATAAAATG).

In vivo experiments

Ethical and operational permission for *in vivo* experiments was granted by the RHUL Animal Welfare Committee and the UK Home Office. This work was conducted under statutory Home Office regulatory, ethics and licensing procedures, under the Animals (Scientific Procedures) Act 1986 (Project Licence 70/8271) C57BL/10 and *mdx* mice were housed with food and water *ad libitum* in minimal disease facilities (Royal Holloway, University of London). Briefly, 8 week old male mice were anesthetised with isoflurane and 5 x 10^{10} viral particles of AAV-shRPL3L or 5 x 10^{11} viral particles of AAV-RPL3L-transgene were diluted in 50 ul saline and intramuscularly injected into the left TA muscle. Saline was intramuscularly injected into the right TA muscle to serve as a contralateral control. At 7 weeks post-injection, mice were anesthetised with an intraperitoneal injection of Pentobarbital/Buprenorphine solution and *in situ* TA muscle electrophysiology was performed. After analysis, mice were culled and TA muscles were excised from tendon to tendon, weighed, mounted in optimal cutting temperature (OCT) compound and frozen in liquid nitrogen-cooled isopentane.

Muscle force measurement

Mice were put under terminal anaesthesia using intraperitoneal injection of a Pentobarbital (60 mg/kg) and Buprenorphine (3mg/kg) solution and contractile properties of TA muscles were analysed by *in situ* muscle electrophysiology using a protocol previously described[24]. Briefly, clamps were used to fix the knee and foot of the mouse and the distal tendon of the TA muscle was attached to a 305B dual-mode servomotor transducer (Aurora Scientific, Aurora, Ontario, Canada) using a 4.0 braided surgical silk (Interfocus, Cambridge, UK). The sciatic nerve of the mouse was proximally cut and stimulated distally by a bipolar silver electrode using supramaximal square wave pulses of 0,02 ms duration (701A stimulator; Aurora Scientific). Isometric measurements were made at an initial length L0 (length at which maximal tension was obtained during the tetanus). Muscle length was measured using a digital calliper.

Response to tetanic stimulation (pulse frequency: 10, 30, 40, 50, 80, 100, 120, 150, 180 Hz) was recorded and the maximal force was determined. A Lab-View-based DMC program (Dynamic muscle control and Data Acquisition; Aurora Scientific) was used to record and analyse data provided by the isometric transducer. Specific force (g/cm^2) was calculated by dividing the maximal tetanic force by TA muscle cross-sectional area estimated using the following formula: muscle weight (g)/[TA fiber length (Lf; cm) × 1.06 (g/cm^3)]. To assess the muscle resistance to eccentric contractions, a lengthening of 10% of muscle was applied for 10 consecutive contractions. Maximal (isometric) force generated after each eccentric contraction is expressed as percentage of to the initial maximal force. After contractile measurements muscles were collected.

Western blot

Protein lysates were prepared by homogenising muscle in RIPA buffer (1% nonidet P-40, 0.5% sodium deoxycholate, 0.1% SDS, 50 mM NaCl, 20 mM Tris-HCl pH 7.6, 1 mM EDTA with complete protease inhibitor cocktail (Sigma-Aldrich) and Pierce phosphatase inhibitor) using 3mm tungsten carbide beads with the TissueLyser system (Qiagen) for whole muscle samples, or by vortexing for muscle sections, followed by centrifugation at 16,000 g at 4°C for 10 minutes. The supernatant was retained and protein concentration was quantified using the DC protein assay (BIO-RAD) with a BSA standard. The protein lysate was denatured in NuPAGE sample reducing agent and LDS sample buffer (Invitrogen) for 10 minutes at 70°C prior to separation by gel electrophoresis. Proteins were separated on 3-8% Tris-Acetate gels (Invitrogen) and transferred onto a 0.25 μm nitrocellulose membrane (GE Healthcare) for 1.5-2 hours at 30 V constant. The membrane was blocked in 5% milk in PBS for 1 hour at room temperature then stained overnight at 4°C with primary antibodies specific for vinculin raised in mouse (Sigma SAB42000080, 1/10,000 dilution), RPL3L raised in rabbit (gift from J.J.

McCarthy, 1/1,000 dilution), RPL3 (Proteintech 11005-1-AP, 1/2,000 dilution), HA raised in rabbit (Abcam ab18181). Membranes were then incubated for 1 hour at room temperature with appropriate secondary antibodies conjugated to LICOR IRDye 800CW (goat anti-mouse IgG (H+L) and goat anti-rabbit IgG (H+L), 1/10,000 dilution). The LI-COR Odyssey Infrared Imaging System was used to detect signals from the membrane, with quantification using LI-COR Image Studio software.

Immunofluorescence staining and muscle histology

Frozen TA muscles were sectioned at 10 μm thickness using an OTF 5000 cryostat (Bright). Tissue sections were collected on coated glass slides (VWR) and stored at -80°C prior to use. For RPL3L/laminin and collagen VI/laminin immunostainings, sections were rehydrated in PBS, blocked with 10% goat serum in PBS tween 0.5% (PBST) for 1h at room temperature (RT). Afterwards sections were incubated with primary antibodies. Slides were stained with primary antibodies for RPL3L (in-house polyclonal rabbit antibody generated by John McCarthy, diluted 1:200), laminin (rat monoclonal, diluted 1:800, Sigma-Aldrich L0663) and collagen VI (rabbit polyclonal, diluted 1:200, Abcam ab6588) for 1h at RT. Secondary antibodies were Alexa-fluor (Life Biotechnologies, Paisley, UK) conjugated to 488 or 594 fluorochromes, diluted 1:200 and used for 1h at RT. Lastly, slides were stained with 1 μg/mL DAPI (Sigma) for 5 minutes at RT, washed, and mounted in Mowiol 4-88 (Sigma). For sirius red staining, slides were air-dried, fixed in 4% PFA, washed in water, dehydrated in 100% ethanol, and air-dried again. Slides were then stained in sirius red solution (0.3% in picric acid) for 1 hour, washed in water, fixed in 0.5% acetic acid, dehydrated in 100% ethanol, cleared in xylene and mounted in DPX mounting medium. Morphometric analyses were performed as previously published[20]. Briefly, myofibre cross sectional area and the percentage of fibres with central nuclei were quantified by taking 5 random fields in the largest section of each

muscles stained with laminin/DAPI and analyses were performed using MuscleJ software[25]. Analyses of area covered by collagen VI or sirius red were performed by taking 5 random fields in sections stained by collagen VI/DAPI or sirius red respectively and quantification was performed using NIH ImageJ analysis software (NIH, Bethesda, Maryland, US). All images were randomly taken from a blinded observer. Slides were imaged using a Nikon Ni-E upright microscope.

Statistical analysis

All data are presented as mean values ± error of the mean (Mean ± S.E.M.). GraphPad Prism (Version 6.07) was used for the analyses. Statistical analyses were performed using the two-tailed t-test, two-tailed paired t-test or two-way ANOVA as appropriate. A difference was considered to be significant at *P<0.05, **P<0.01, ***P<0.001 or ****P<0.0001.

Acknowledgements

B.R.K. was funded by the Neurological Foundation of New Zealand. The authors thank Benitec Biopharma for designing shRNAs targeting RPL3L, Ornella Cappellari for assistance with *in vivo* muscle electrophysiology, and Emma Popescu and Nicola Sanderson for care and maintenance of animals.

Author Contributions

Conceptualisation, B.R.K., L.J.P., and G.D.; Methodology, B.R.K, N.B.L-N and A.M.; Validation, B.R.K., N.B.L-N, P.H. and A.M.; Formal Analysis, B.R.K. N.B.L-N, P.H. and A.M.; Investigation, B.R.K., N.B.L-N., A.M.; Resources, J.J.M.; Writing – Original Draft, B.R.K.; Writing – Review and Editing, B.R.K., A.M., N.B.L-N., J.J.M., L.J.P. and G.D.; Visualisation, B.R.K.; Supervision, L.J.P. and G.D.; Project Administration, L.J.P and G.D.; Funding Acquisition, B.R.K, L.J.P and G.D.

Figure legends

Figure 1: Developmental expression of RPL3L and RPL3. (A) Western blot for RPL3L, RPL3 and vinculin on TA muscle protein lysate collected from C57 and *mdx* mice aged 1 day, 3 days, 1 week, 2 weeks and 8 weeks. (B-C) Quantification of the protein signals of RPL3L and RPL3 were normalised to vinculin as the protein loading control. The expression profile of RPL3L and RPL3 showed an inverse relationship. (D) immunostaining for RPL3L (red) and laminin (Green). Nuclei are counterstained with DAPI (blue). TA muscles of 4 and 8 week old C57 and *mdx* mice were analysed. Scale bar, 100 μm. In B and C data are presented as mean values ± error of the mean (Mean ± S.E.M.) of 3 biological replicates. Statistical analysis was performed using the two-tailed paired t-test (*P<0.05, **P<0.01, ***P<0.001).

Figure 2: *In situ* TA muscle electrophysiology following RPL3L knockdown in C57 and *mdx*. (A and B) Specific force measures at 150Hz stimulation in TA muscles at 7 weeks post-injection with saline (Ctrl) compared to AAV to knockdown RPL3L (KD). A significant increase in specific force following RPL3L knockdown is observed in both C57 (A) and *mdx* (B) mice. (C) Eccentric contractions in *mdx* over 11 repetitions showed a decrease in force as a percentage of maximal force. Data are presented as Mean ± S.E.M. of 8 or 6 biological replicates for C57 and *mdx* respectively. Statistical analysis was performed using the two-way ANOVA or two-tailed paired t-test as appropriate (*P<0.05, **P<0.01, ***P<0.001, ****P<0.0001).

Figure 3: RPL3L knockdown in C57 and *mdx*. (A and C) Western blot for RPL3L and vinculin on TA muscle protein lysate collected from C57 (A) and *mdx* (C) mice at 7-weeks

post injection with saline (Ctrl) compared to AAV to knockdown RPL3L (KD). (B and D) Quantification of the protein signal of RPL3L was normalised to vinculin as the protein loading control. Protein expression of RPL3L was significantly reduced by shRNA knockdown of RPL3L compared to the control in both C57 and *mdx*. (E-F) Immunofluorescence staining for laminin/DAPI and RPL3L in sections of C57 (E) and *mdx* (F) mice with or without RPL3L knockdown. Scale bar, 200 μm. (G-N) Measurements of TA cross sectional area (CSA) (G-H), myofibre CSA in TA muscle (I-L), and TA muscle length (M-N) at 7 weeks post-injection in Ctrl compared to KD in C57 (G, I, M) and *mdx* (H, L, N) mice. A significant increase in TA length following RPL3L knockdown is observed in both C57 (M) and *mdx* (N). Data are presented as Mean ± S.E.M. of 8 or 6 biological replicates for C57 and *mdx* respectively. Statistical analysis was performed using the two-tailed unpaired t-test (*P<0.05, **P<0.01, ns: not significant).

Supplementary data

Supplementary figure 1: Assessment of fibrosis in TA muscles of 4 and 8 week old C57 and *mdx* mice. Upper panel: immunostaining for collagen VI (green) and DAPI (blue) in C57 and *mdx* TA muscles of 4 and 8 week old mice. Lower panel: sirius red staining (red) of collagen proteins in C57 and *mdx* TA muscles of 4 and 8 week old mice. Scale bar, 200 μm. More fibrosis is detected in *mdx* muscles at both time points.

Supplementary figure 2: Overexpression of RPL3L in C57 and *mdx* mice. (A) Western blotting for RPL3L, HA and vinculin was conducted on TA muscle lysates from C57 mice treated with saline (Ctrl) or the RPL3L overexpression (OE) construct which was tagged with hemagglutinin (HA). Vinculin was used as the protein loading control. (B) Quantification of

HA and RPL3L by densitometric analysis of the WB. (C-E) *In vivo* muscle electrophysiology to measure specific force in TA muscles of C57 (C) and *mdx* (D) mice and resistance to eccentric contractions (E) over 11 repetitions conducted on the TA muscle *mdx* mice treated with saline (Ctrl) or the AAV-RPL3L (OE) construct. (F-M) Parameters measured in TA muscles from C57 and *mdx* mice treated with saline or the AAV-RPL3L construct: length, (F) mass (G) and CSA (H) measurements of TA muscles of C57 mice. Length, (I) mass (L) and CSA (M) measurements of TA muscle of *mdx* mice. Data are presented as Mean ± S.E.M. Statistical analysis was performed using the two-way ANOVA or two-tailed paired t-test as appropriate; ***P<0.001, ns: not significant).

Supplementary figure 3: assessment of fibrosis in TA muscles of mdx mice treated with saline (Ctrl) or AAV-shRPL3L (KD). (A) laminin (green), DAPI (blue) and collagen VI (red) immunostaining in sections of TA muscles of mdx mice treated with saline or AAV-shRPL3L. A similar amount of collagen VI is detected after either treatments. (B) Percentage of fibres with centralised nuclei. No difference was detected after either treatment. (C) The percentage of area covered by collagen VI in TA muscle sections of mdx mice is similar after injection of either saline or AAV-shRPL3L. (D) Sirius red staining in sections of TA muscles of *mdx* mice treated with saline or AAV-shRPL3L. Similar amounts of collagen proteins are detected after either treatments. (E) Percentage of area covered by collagen proteins (detected by sirius red) in TA muscle sections of *mdx* mice is similar after injection of either saline or AAV-shRPL3L. Scale bar, 200 µm. Data are presented as Mean ± S.E.M. Statistical analysis was performed using the two-tailed paired t-test; ns: not significant).

References

1 Van Raay TJ, TD Connors, KW Klinger, GM Landes and TC Burn. (1996). A novel ribosomal protein L3-like gene (RPL3L) maps to the autosomal dominant polycystic kidney disease gene region. Genomics 37:172-176.

2 Schulze H and KH Nierhaus. (1982). Minimal set of ribosomal components for reconstitution of the peptidyltransferase activity. EMBO J 1:609-613.

3 Venema J and D Tollervey. (1999). Ribosome synthesis in Saccharomyces cerevisiae. Annu Rev Genet 33:261-311.

4 Thorrez L, K Van Deun, LC Tranchevent, L Van Lommel, K Engelen, K Marchal, Y Moreau, I Van Mechelen and F Schuit. (2008). Using ribosomal protein genes as reference: a tale of caution. PloS one 3:e1854.

5 Gupta V and JR Warner. (2014). Ribosome-omics of the human ribosome. RNA 20:1004-1013.

6 Ganapathi M, L Argyriou, F Martinez-Azorin, S Morlot, G Yigit, TM Lee, B Auber, A von Gise, DS Petrey, H Thiele *et al.* (2020). Bi-allelic missense disease-causing variants in RPL3L associate neonatal dilated cardiomyopathy with muscle-specific ribosome biogenesis. Hum Genet 139:1443-1454.

7 Chaillou T, X Zhang and JJ McCarthy. (2016). Expression of Muscle-Specific Ribosomal Protein L3-Like Impairs Myotube Growth. J Cell Physiol 231:1894-1902.

8 Chen YW, P Zhao, R Borup and EP Hoffman. (2000). Expression profiling in the muscular dystrophies: identification of novel aspects of molecular pathophysiology. J Cell Biol 151:1321-1336.

9 Haslett JN, D Sanoudou, AT Kho, RR Bennett, SA Greenberg, IS Kohane, AH Beggs and LM Kunkel. (2002). Gene expression comparison of biopsies from Duchenne muscular dystrophy (DMD) and normal skeletal muscle. Proc Natl Acad Sci U S A 99:15000-15005.

10 Seno MM, C Trollet, T Athanasopoulos, IR Graham, P Hu and G Dickson. (2010). Transcriptomic analysis of dystrophin RNAi knockdown reveals a central role for dystrophin in muscle differentiation and contractile apparatus organization. BMC genomics 11:345.

11 Mendell JR and M Lloyd-Puryear. (2013). Report of MDA muscle disease symposium on newborn screening for Duchenne muscular dystrophy. Muscle Nerve 48:21-26.

12 Gumerson JD and DE Michele. (2011). The dystrophin-glycoprotein complex in the prevention of muscle damage. J Biomed Biotechnol 2011:210797.

13 Matsumura K, K Ohlendieck, VV Ionasescu, FM Tome, I Nonaka, AH Burghes, M Mora, JC Kaplan, M Fardeau and KP Campbell. (1993). The role of the dystrophin-glycoprotein complex in the molecular pathogenesis of muscular dystrophies. Neuromuscular disorders : NMD 3:533-535.

14 Duan D. (2018). Systemic AAV Micro-dystrophin Gene Therapy for Duchenne Muscular Dystrophy. Mol Ther 26:2337-2356.

15 Head SI, DA Williams and DG Stephenson. (1992). Abnormalities in structure and function of limb skeletal muscle fibres of dystrophic mdx mice. Proc Biol Sci 248:163-169.

16 Moens P, PH Baatsen and G Marechal. (1993). Increased susceptibility of EDL muscles from mdx mice to damage induced by contractions with stretch. J Muscle Res Cell Motil 14:446-451.

17 Lee SJ. (2004). Regulation of muscle mass by myostatin. Annu Rev Cell Dev Biol 20:61-86.

18 Mariot V, R Joubert, C Hourde, L Feasson, M Hanna, F Muntoni, T Maisonobe, L Servais, C Bogni, R Le Panse *et al.* (2017). Downregulation of myostatin pathway in neuromuscular diseases may explain challenges of anti-myostatin therapeutic approaches. Nat Commun 8:1859.

19 Lu-Nguyen N, G Dickson and A Malerba. (2018). Systemic Intravenous Administration of Antisense Therapeutics for Combinatorial Dystrophin and Myostatin Exon Splice Modulation. Methods Mol Biol 1828:343-354.

20 Lu-Nguyen N, A Ferry, FJ Schnell, GJ Hanson, L Popplewell, G Dickson and A Malerba. (2019). Functional muscle recovery following dystrophin and myostatin exon splice modulation in aged mdx mice. Hum Mol Genet 28:3091-3100.

21 Lu-Nguyen N, A Malerba, L Popplewell, F Schnell, G Hanson and G Dickson. (2017). Systemic Antisense Therapeutics for Dystrophin and Myostatin Exon Splice Modulation Improve Muscle Pathology of Adult mdx Mice. Mol Ther Nucleic Acids 6:15-28.

22 Malerba A, JK Kang, G McClorey, AF Saleh, L Popplewell, MJ Gait, MJ Wood and G Dickson. (2012). Dual Myostatin and Dystrophin Exon Skipping by Morpholino Nucleic Acid Oligomers Conjugated to a Cell-penetrating Peptide Is a Promising Therapeutic Strategy for the Treatment of Duchenne Muscular Dystrophy. Mol Ther Nucleic Acids 1:e62.

23 Tonino P, B Kiss, J Strom, M Methawasin, JE Smith, 3rd, J Kolb, S Labeit and H Granzier. (2017). The giant protein titin regulates the length of the striated muscle thick filament. Nat Commun 8:1041.

24 Malerba A, P Klein, H Bachtarzi, SA Jarmin, G Cordova, A Ferry, V Strings, MP Espinoza, K Mamchaoui, SC Blumen *et al.* (2017). PABPN1 gene therapy for oculopharyngeal muscular dystrophy. Nat Commun 8:14848.

25 Mayeuf-Louchart A, D Hardy, Q Thorel, P Roux, L Gueniot, D Briand, A Mazeraud, A Bougle, SL Shorte, B Staels *et al.* (2018). MuscleJ: a high-content analysis method to study skeletal muscle with a new Fiji tool. Skelet Muscle 8:25.

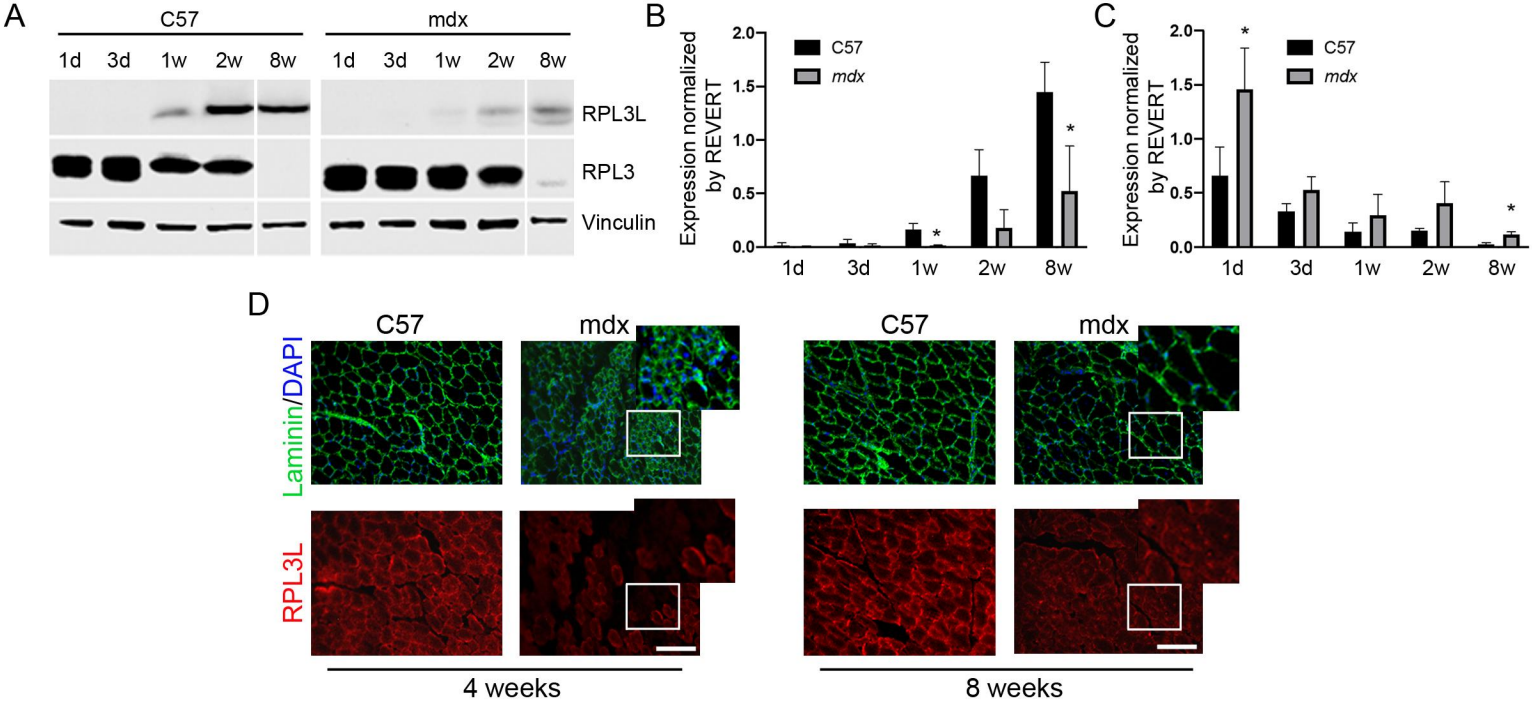
A
C57
mdx
1d 3d 1w 2w 8w
1d 3d 1w 2w 8w
RPL3L
RPL3
Vinculin
B
Expression normalized by REVERT
C57
mdx
2.0
1.5
1.0
0.5
0.0
1d 3d 1w 2w 8w
C
Expression normalized by REVERT
C57
mdx
2.0
1.5
1.0
0.5
0.0
1d 3d 1w 2w 8w
D
C57
mdx
C57
mdx
Laminin/DAPI
RPL3L
4 weeks
8 weeks

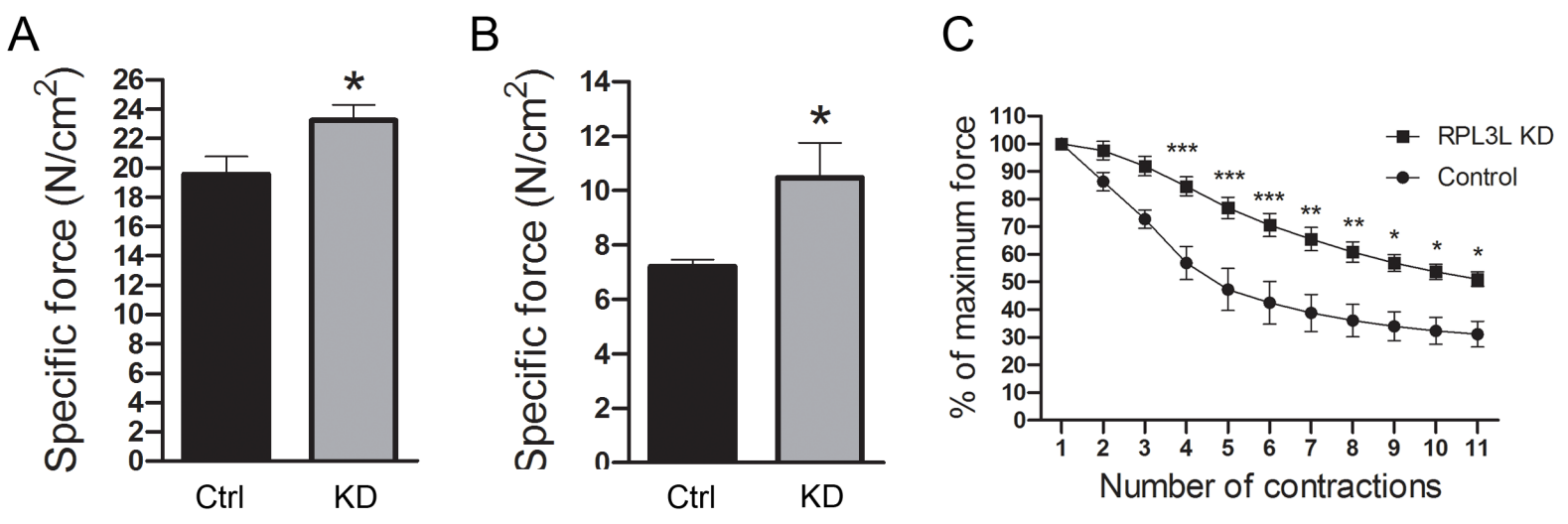
A
Specific force (N/cm2)
26
24
22
20
18
16
14
12
10
8
6
4
2
0
*
Ctrl
KD
B
Specific force (N/cm2)
14
12
10
8
6
4
2
0
*
Ctrl
KD
C
% of maximum force
110
100
90
80
70
60
50
40
30
20
10
0
***
***
***
**
**
*
*
*
RPL3L KD
Control
1
2
3
4
5
6
7
8
9
10
11
Number of contractions

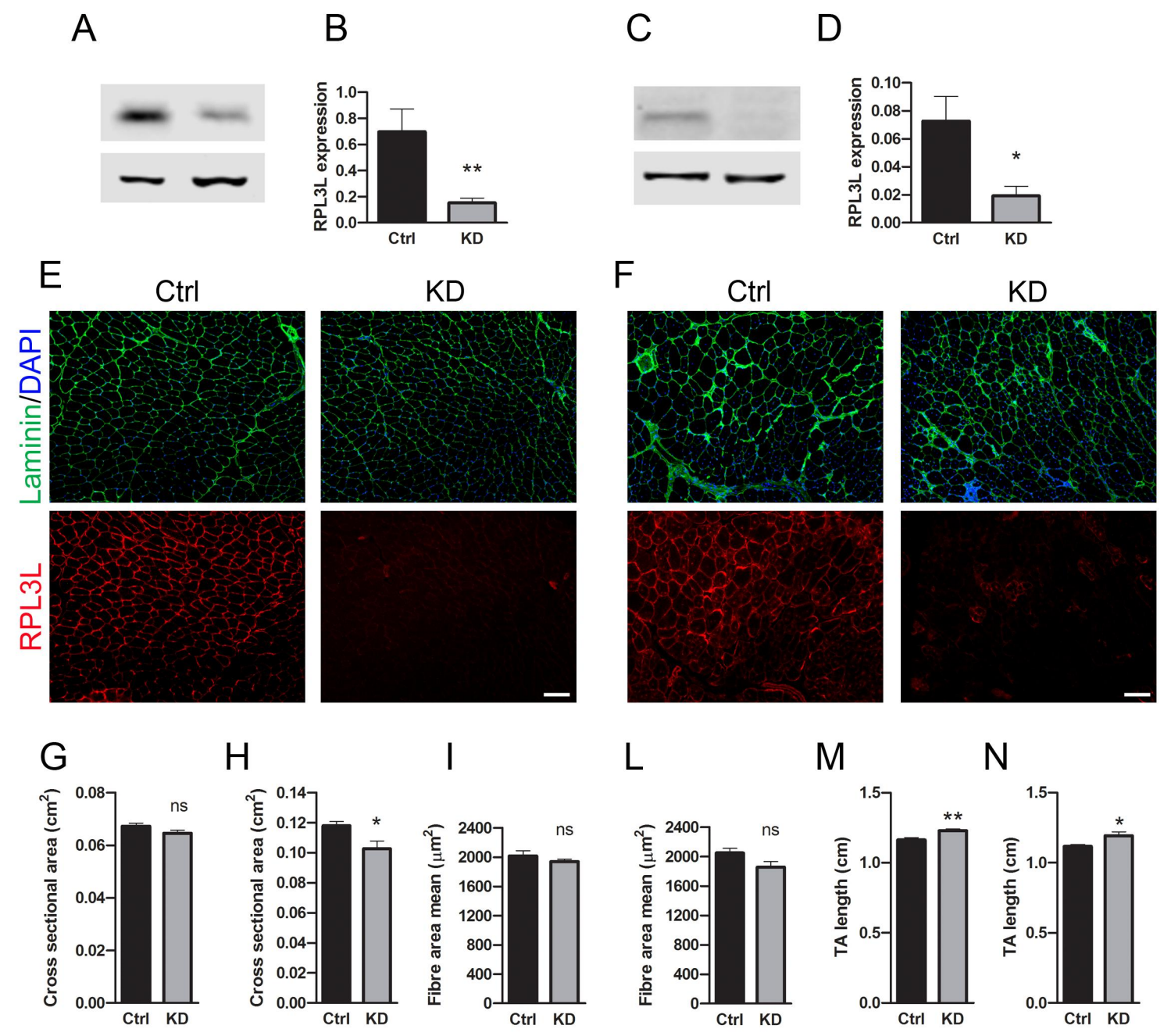
A
B
RPL3L expression
1.0
0.8
0.6
0.4
0.2
0.0
**
Ctrl
KD
C
D
RPL3L expression
0.10
0.08
0.06
0.04
0.02
0.00
*
Ctrl
KD
E
Ctrl
KD
Laminin/DAPI
RPL3L
F
Ctrl
KD
G
Cross sectional area (cm2)
0.08
0.06
0.04
0.02
0.00
ns
Ctrl
KD
H
Cross sectional area (cm2)
0.14
0.12
0.10
0.08
0.06
0.04
0.02
0.00
*
Ctrl
KD
I
Fibre area mean (μm2)
2400
2000
1600
1200
800
400
0
ns
Ctrl
KD
L
Fibre area mean (μm2)
2400
2000
1600
1200
800
400
0
ns
Ctrl
KD
M
TA length (cm)
1.5
1.0
0.5
0.0
**
Ctrl
KD
N
TA length (cm)
1.5
1.0
0.5
0.0
*
Ctrl
KD

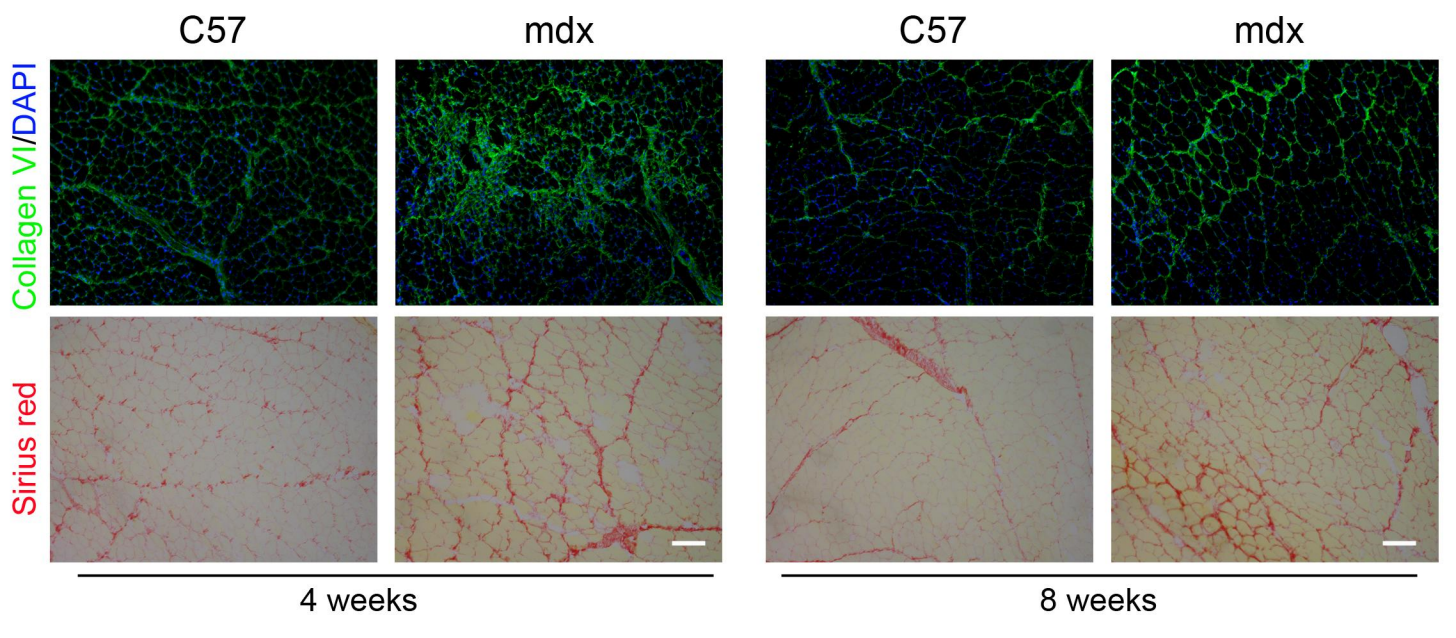
C57
mdx
C57
mdx
Collagen VI/DAPI
Sirius red
4 weeks
8 weeks

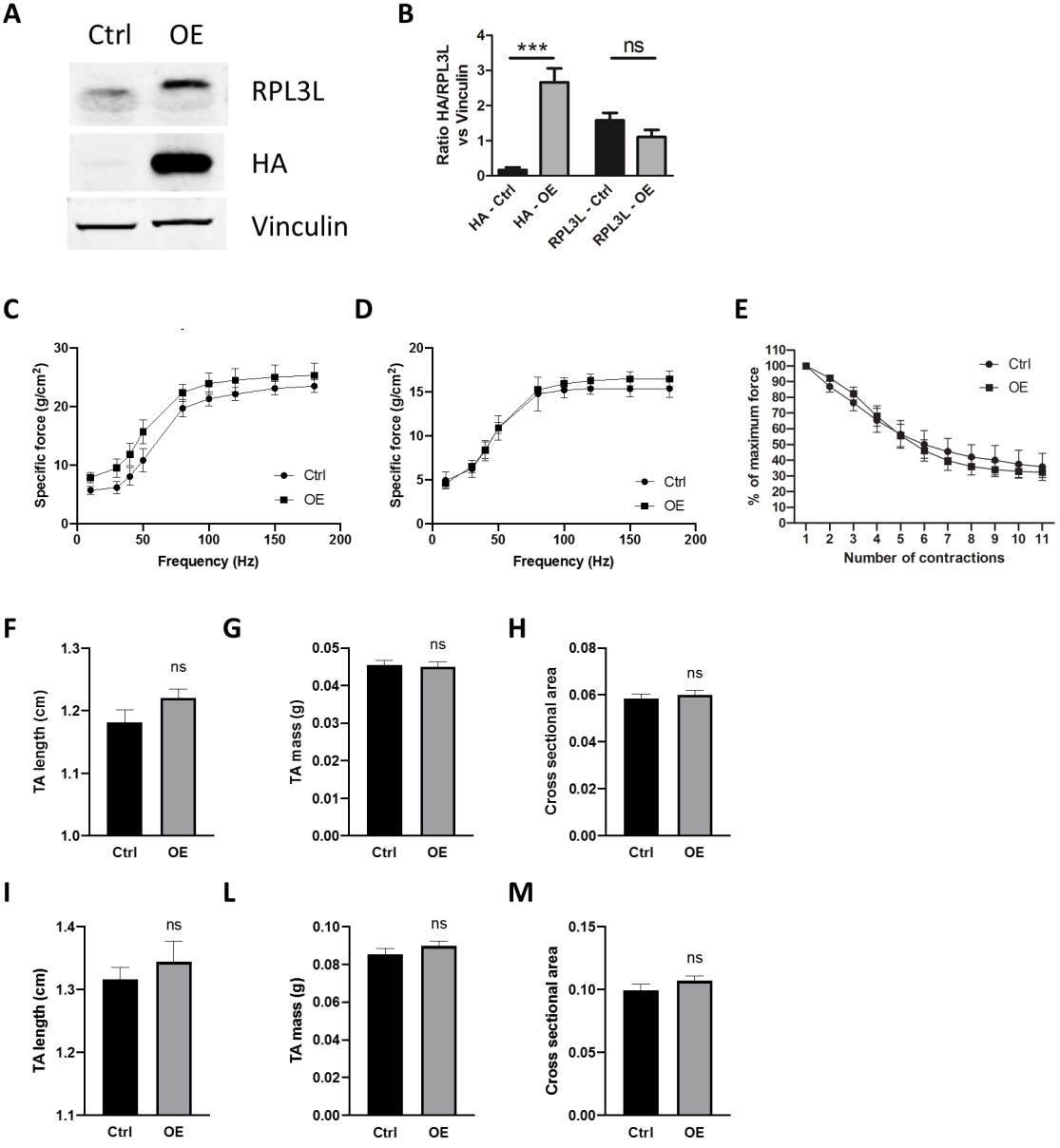
A
Ctrl
OE
RPL3L
HA
Vinculin
B
Ratio HA/RPL3L vs Vinculin
***
ns
HA - Ctrl
HA - OE
RPL3L - Ctrl
RPL3L - OE
C
Specific force (g/cm²)
Frequency (Hz)
Ctrl
OE
D
Specific force (g/cm²)
Frequency (Hz)
Ctrl
OE
E
% of maximum force
Number of contractions
Ctrl
OE
F
TA length (cm)
ns
Ctrl
OE
G
TA mass (g)
ns
Ctrl
OE
H
Cross sectional area
ns
Ctrl
OE
I
TA length (cm)
ns
Ctrl
OE
L
TA mass (g)
ns
Ctrl
OE
M
Cross sectional area
ns
Ctrl
OE

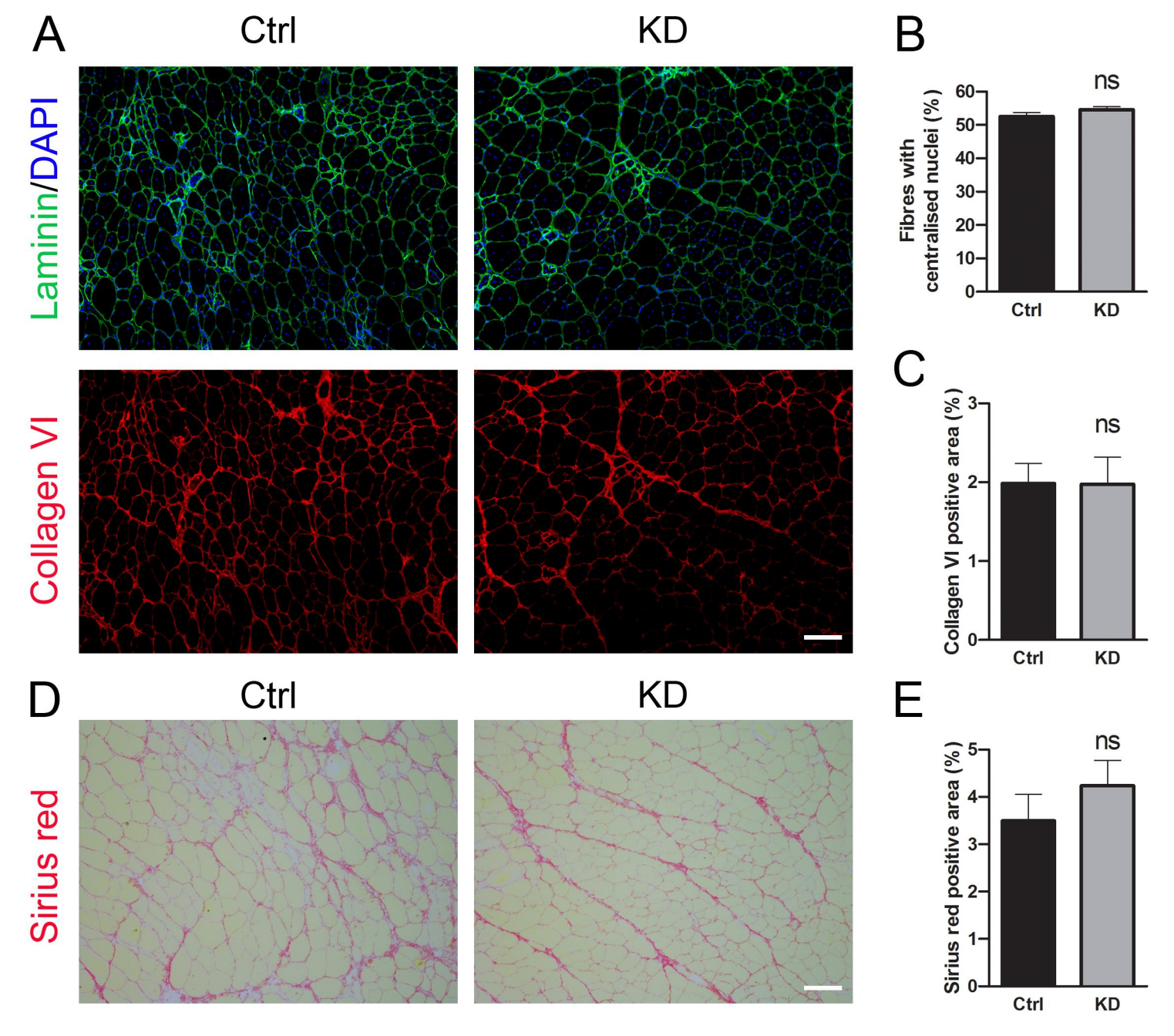
A
Ctrl
KD
Laminin/DAPI
Collagen VI
B
ns
Fibres with centralised nuclei (%)
60
50
40
30
20
10
0
Ctrl
KD
C
ns
Collagen VI positive area (%)
3
2
1
0
Ctrl
KD
D
Ctrl
KD
Sirius red
E
ns
Sirius red positive area (%)
5
4
3
2
1
0
Ctrl
KD